

Thick-target inverse-kinematics proton scattering from ^{46}Ar and the $N = 28$ shell below ^{48}Ca

L. A. Riley,¹ M. A. Abdelqader,¹ D. Bazin,² M. J. Bojazi,¹ B. A. Brown,^{2,3} C. M. Campbell,^{2,3} J. A. Church,^{2,3,*} P. D. Cottle,⁴ D.-C. Dinca,^{2,3} J. Enders,^{2,†} A. Gade,² T. Glasmacher,^{2,3} M. Honma,⁵ S. Horibe,⁶ Z. Hu,² K. W. Kemper,⁴ W. F. Mueller,² H. Olliver,^{2,3} T. Otsuka,^{7,8} B. C. Perry,^{2,3} B. T. Roeder,⁴ B. M. Sherrill,^{2,3} T. P. Spencer,¹ and J. R. Terry^{2,3}

¹*Department of Physics and Astronomy, Ursinus College, Collegeville, Pennsylvania 19426, USA*

²*National Superconducting Cyclotron Laboratory, Michigan State University, East Lansing, Michigan 48824, USA*

³*Department of Physics and Astronomy, Michigan State University, East Lansing, Michigan 48824, USA*

⁴*Department of Physics, Florida State University, Tallahassee, Florida 32306, USA*

⁵*Center for Mathematical Sciences, University of Aizu, Tsuruga, Ikki-machi, Aizu-Wakamatsu, Fukushima 965-8580, Japan*

⁶*Department of Physics and Astronomy, Earlham College, Richmond, Indiana 47374, USA*

⁷*Department of Physics and Center for Nuclear Study, University of Tokyo, Hongo, Tokyo 113-0033, Japan*

⁸*RIKEN, Hirosawa, Wako-shi, Saitama 351-0198, Japan*

(Received 28 March 2005; published 17 August 2005)

Low-lying excited states of ^{46}Ar have been studied via inverse-kinematics proton scattering with a thick target. Coupled-channels calculations have been used to extract the deformation length of the 2_1^+ state. This result, combined with existing Coulomb excitation data, yields a ratio of the neutron-to-proton transition matrix elements of $M_n/M_p = 1.19(25)N/Z$, showing a departure from the proton dominance observed in the $N = 28$ isotones above ^{48}Ca . The status of the $N = 28$ shell below ^{48}Ca is discussed.

DOI: 10.1103/PhysRevC.72.024311

PACS number(s): 25.40.Ep, 21.10.Re

I. INTRODUCTION

A wealth of theoretical work exists in the literature on the status of the $N = 28$ shell below ^{48}Ca . Mean field calculations [1–5] predict a strongly quadrupole-deformed ground state for ^{44}S and a very shallow oblate minimum in the potential energy surface for ^{46}Ar . Shell model calculations [6–9] indicate only weak, if any, erosion of the $N = 28$ shell. They reproduce the experimentally observed 2_1^+ excitation energies, but yield $B(E2)$ values for ^{46}Ar which are too large by a factor of roughly 2. Despite the increase of approximately 400 keV in 2_1^+ excitation energies from $N = 26$ to $N = 28$ in the sulfur and argon isotopes and a drop in the slope of the two-neutron separation energy S_{2N} in the argon isotopes at $N = 28$ [9], there is some experimental evidence for the breaking of the $N = 28$ shell below ^{48}Ca . A deformed ground state of ^{44}S is indicated by β -decay studies [10,11], and the excitation strength of the 2_1^+ state of $B(E2; 0_{\text{g.s.}}^+ \rightarrow 2_1^+) = 314(88) e^2 \text{ fm}^4$ measured via Coulomb excitation [12] of ^{44}S is not significantly below those of the neighboring sulfur isotopes $^{40,42}\text{S}$. However, in ^{46}Ar , the excitation strength $B(E2; 0_{\text{g.s.}}^+ \rightarrow 2_1^+) = 218(31) e^2 \text{ fm}^4$ of the 2_1^+ state, measured via Coulomb excitation [13], is significantly lower than that of the 2_1^+ states of the neighboring neutron-rich argon isotopes $^{40,42,44}\text{Ar}$, all of which have values above $300 e^2 \text{ fm}^4$ [14,15]. This could be attributed to the persistence of the $N = 28$ shell in ^{46}Ar . However, an electromagnetic probe such as Coulomb excitation only provides the proton transition matrix element

M_p . A comparison of the neutron and proton transition matrix elements can further clarify the status of the $N = 28$ shell in ^{46}Ar .

The ratio of neutron to proton transition matrix elements is related to the neutron and proton deformation lengths δ_n and δ_p via [16]

$$\frac{M_n}{M_p} = \frac{N\delta_n}{Z\delta_p}. \quad (1)$$

In the simplest picture of low-lying collective excitations, protons and neutrons have equal deformation lengths, and hence we expect $M_n/M_p = N/Z$. However, shell structure leads to departures from this simple prediction. As was first pointed out by Bernstein, Brown, and Madsen [16,17], in a nucleus with a closed neutron (proton) shell, we expect valence protons (neutrons) to dominate low-lying collective excitations, which should therefore have $M_n/M_p > N/Z$ ($M_n/M_p < N/Z$). Deformation lengths measured with a pair of complementary experimental probes having different sensitivities to protons and neutrons can be combined to obtain M_n/M_p . This approach has been shown to be a reliable indicator of shell closure over a broad range of single-closed-shell nuclei [16–18].

The advent of radioactive beams has made it possible to perform both Coulomb excitation [19,20] and proton scattering in inverse kinematics [21,22] at intermediate beam energies. Hence, it is now possible to disentangle proton and neutron contributions to low-lying excited states of exotic nuclei. Inverse-kinematics proton-scattering measurements have typically involved detection of scattered protons in coincidence with recoiling beam particles. A thin target must be used in order to limit the angular straggling of the scattered protons, effectively placing a lower limit on beam intensity

*Present address: Lawrence Livermore National Laboratory, Livermore, CA 94550.

†Present address: Institut für Kernphysik, TU Darmstadt, D-64289 Darmstadt, Germany.

on the order of 10^4 pps. A thick-target technique has been introduced by Iwasaki *et al.* [23] in which position-sensitive γ -ray detectors are used to measure inelastic scattering in coincidence with recoiling beam particles. This technique affords superior energy resolution and can extend the reach of proton-scattering measurements to beam intensities on the order of 10^3 pps. Moreover, deexcitation γ rays can reveal the presence of intermediate states not directly populated by the reaction, providing additional information about the level structure.

In the present work, we present a thick-target inverse-kinematics proton-scattering measurement of the quadrupole deformation length of the $0_{g.s.}^+ \rightarrow 2_1^+$ excitation of ^{46}Ar and combine our result with the most recent Coulomb excitation result [13] to obtain M_n/M_p . A variety of measurements have yielded $M_n/M_p < N/Z$ for the 2_1^+ states of ^{50}Ti , ^{52}Cr , and ^{54}Fe , the stable even-even $N = 28$ isotones above ^{48}Ca [16,17]. However, our result of $M_n/M_p = 1.19(25)N/Z$ for the 2_1^+ state of ^{46}Ar indicates a greater neutron contribution to the excitation. We discuss the status of the $N = 28$ shell at $Z = 18$ in light of this result. In addition, we tentatively identify the 3_1^- state and extract the octupole deformation length of the $0_{g.s.}^+ \rightarrow 3_1^-$ excitation.

II. EXPERIMENT

The experiment was performed at the Coupled Cyclotron Facility of the National Superconducting Cyclotron Laboratory at Michigan State University. A 110 MeV/nucleon ^{48}Ca primary beam was fragmented on a 376 mg/cm² ^9Be primary target at the midacceptance target position of the A1900 fragment separator [24]. The momentum acceptance of the A1900 was set to 0.5%. A secondary beam of ^{46}Ar fragments, with an energy of 76.4 MeV/nucleon, an intensity of 8300 pps, and a purity of about 99%, was incident on 191 mg/cm² polypropylene [$(\text{C}_3\text{H}_6)_n$] and 211 mg/cm² graphite secondary targets at the target position of the S800 magnetic spectrograph [25], which was used to identify and determine the scattering angles of beam particles on an event-by-event basis. Data were collected for approximately 9.3 h with the polypropylene target and 3.6 h with the carbon target.

Deexcitation γ rays were detected by SeGA (segmented germanium array), an array of fifteen 32-fold segmented coaxial HPGe detectors [26] arranged in two rings centered at 37° and 90° relative to the beam axis. The centers of the detectors were 24 cm from the center of the secondary target. The segmentation of SeGA enabled event-by-event Doppler reconstruction of γ -ray energy spectra in the reference frame of the scattered projectiles. The scattered beam velocities used in the Doppler reconstruction of γ -ray spectra were varied to match the centroids of the 1558 keV photopeaks in the spectra collected by the 37° and 90° rings of SeGA. Velocities of $v/c = 0.362(1)$ and $v/c = 0.365(1)$ were determined by this method for the polypropylene and graphite targets, respectively. These correspond to midtarget beam energies of 68 MeV/nucleon in the polypropylene target and 69 MeV/nucleon in the graphite target. Prompt and nonprompt γ -ray spectra were produced

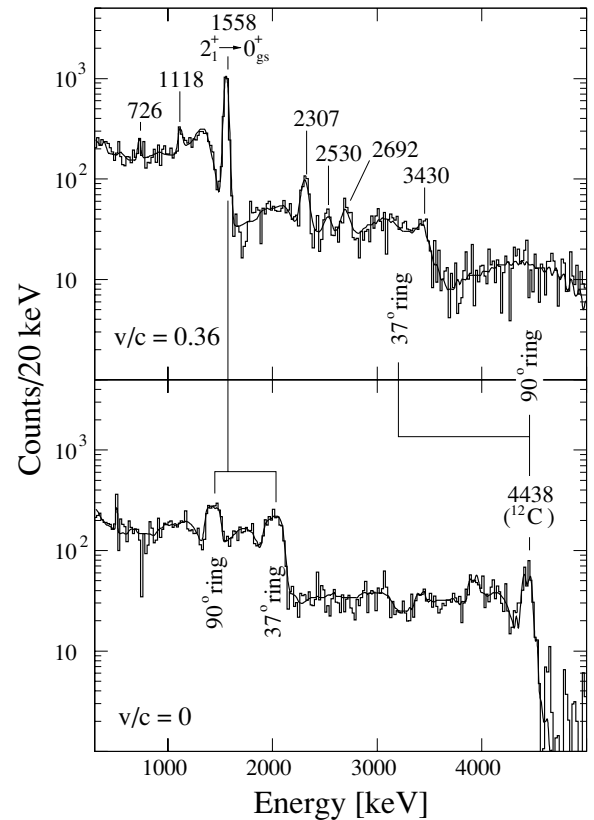


FIG. 1. Background-subtracted γ -ray spectra measured in coincidence with ^{46}Ar particles scattered from the 191 mg/cm² polypropylene target. Top panel shows Doppler-corrected spectrum ($v/c = 0.36$); bottom panel, laboratory-frame spectrum ($v/c = 0$). GEANT3-fit spectrum appears as a solid curve in each panel.

via software gating on particle- γ timing spectra. Each prompt gate was 150 ns wide, and the corresponding nonprompt gate was a combination of portions of the timing spectrum to either side of the prompt gate having a total width of 150 ns. The nonprompt γ -ray spectra contained no discernible peaks and were produced for the purpose of subtracting the random component of the background in the fitting process, described in detail below. Background-subtracted laboratory-frame ($v/c = 0$) and projectile-frame ($v/c = 0.36$) γ -ray spectra measured in coincidence with ^{46}Ar particles scattered from the polypropylene target are shown in Fig. 1. These spectra correspond to 2.67×10^8 incident ^{46}Ar particles. The spectra arising from 1.03×10^8 ^{46}Ar particles incident on the graphite target are shown in Fig. 2.

III. ANALYSIS AND RESULTS

GEANT3 [27] simulations of the SeGA response were used to extract total γ -ray yields from the measured spectra. The simulations successfully predict photopeak efficiencies obtained from stationary calibration sources within 5%. Simulations of the γ rays observed in the projectile frame, and the 4438 keV peak in the laboratory-frame spectrum, corresponding to the $2_1^+ \rightarrow 0_{g.s.}^+$ transition of ^{12}C , were included in

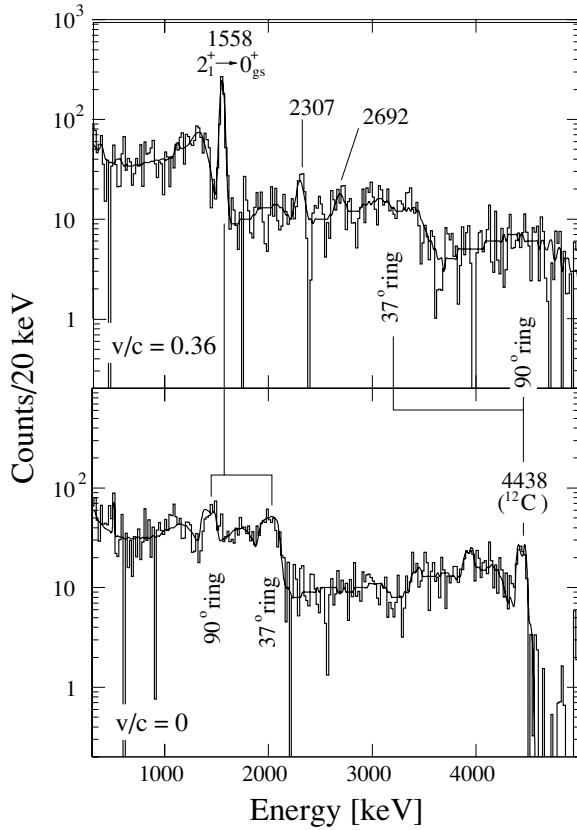


FIG. 2. Same as Fig. 1, but for the 211 mg/cm² graphite target.

the fitting process. For each γ ray, a separate simulation of the response of SeGA to 10^7 events was produced. A linear combination of these simulated spectra, the measured background spectrum, and an exponential function were fit to the measured prompt γ -ray spectrum. The exponential function was included to account for the empirically observed prompt component of the background. The coefficients of the linear combination and the parameters of the exponential function were varied using a log-likelihood maximization procedure to obtain a best fit. The resulting fits are shown as solid curves in both the projectile- and laboratory-frame spectra in Figs. 1 and 2. The cross section for producing each γ ray with the graphite target was used to correct the corresponding cross section measured with the polypropylene target to obtain the proton-scattering cross section. In addition, spectra gated on scattering-angle slices were fit to produce angular distributions of inelastically scattered ^{46}Ar particles discussed below.

Seven peaks corresponding to γ -ray energies of 726(5), 1118(7), 1558(9), 2307(13), 2530(16), 2692(16), and 3430(26) keV are evident in the projectile-frame spectrum of Fig. 1. The 1558 keV γ ray, the dominant peak in the spectrum, corresponds to the $2_1^+ \rightarrow 0_{\text{g.s.}}^+$ transition. The energy obtained here is in reasonable agreement with that of the majority of published measurements [13,15,28,29] but discrepant with the value of 1577(1) keV obtained via deep inelastic heavy-ion scattering [30]. We place the observed γ rays in the proposed level scheme shown in Fig. 3. Energies

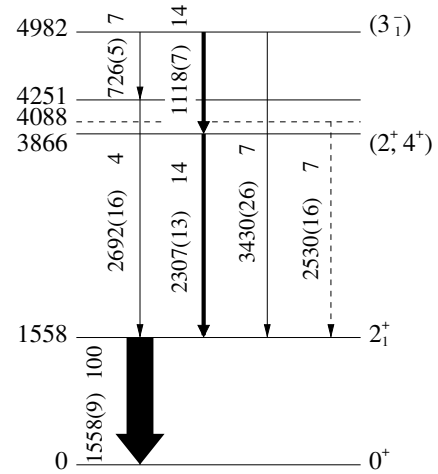


FIG. 3. Proposed level scheme of ^{46}Ar with γ -ray energies and relative intensities from the present work.

and relative intensities of deexcitation γ rays, deduced level energies, and branching ratios are listed in Table I. The 1118 keV γ ray likely corresponds to the 1140 keV transition seen in coincidence with the $2_1^+ \rightarrow 0_{\text{g.s.}}^+$ transition in the fragmentation study of Ref. [28], and the 2307 and 2692 keV γ rays likely correspond to the 2322 and 2710 keV γ rays observed in the same study. Yields of the 726, 1118, 2307, 2692, and 3430 keV γ rays detected in events with a γ -ray multiplicity of two support the placement of the corresponding transitions above the $2_1^+ \rightarrow 0_{\text{g.s.}}^+$ transition in the level scheme. The multiplicity-three yields of the 1118, 1558, and 2307 keV γ rays are significantly above the levels expected because of coincidences with background γ rays, while those of the 726 and 2692 keV γ rays are not large enough to determine whether they are involved in three-step cascades. On the basis of energy sums, we place the 1118–2307 and 726–2692 keV cascades parallel to the 3430 keV transition, and multiplicity gating indicates that this parallel structure feeds the 2_1^+ directly. The energy of the level at 4982(12) keV is the uncertainty-weighted average of the energy sums of the 1118–2307–1558 keV, 726–2692–1558 keV and 3430–1558 keV cascades. The states most strongly populated by inelastic proton scattering are typically low-lying, collective quadrupole and octupole excitations (for example, see Refs. [31–34]). We suggest an assignment of $J^\pi = 3^-$ for the level at 4982 keV based on the strength

TABLE I. Energies of deexcitation γ rays, intensities relative to that of the $2_1^+ \rightarrow 0_{\text{g.s.}}^+$ transition, deduced level energies, and branching ratios from the present work.

E_{level} (keV)	E_γ (keV)	I_γ (%)	Branching ratio (%)
1558(9)	1558(9)	100	100
3866(16)	2307(13)	14(4)	100
4088(18)	2530(16)	7.2(26)	100
4251(18)	2692(16)	4.4(36)	100
4982(12)	726(5)	7.1(18)	25(6)
	1118(7)	14(4)	50(9)
	3430(26)	6.9(35)	25(9)

with which it is populated, but we cannot exclude possible $J^\pi = 2^+, 4^+$ assignments. In Ref. [28], an angular anisotropy measurement of the 2322 keV γ ray (corresponding to the 2307 keV γ ray observed in the present work) indicates a ΔJ of 0 or 2 for this transition, and it was placed above the 2_1^+ level on the basis of γ -ray multiplicity. Based on systematics, we expect the intermediate state populated by a two-step cascade connecting a 3_1^- level to a 2_1^+ level to have either $J^\pi = 2^+$ or $J^\pi = 4^+$. The assignment of ΔJ of 0 or 2 to the 2307 keV is consistent only with the bottom member of such a cascade, leading to the ordering of the 1118–2307 cascade and the assignment of $J^\pi = (2^+, 4^+)$ to the level at 3866 keV. We place the 2692 keV below the 726 keV transition in the 726–2692 keV cascade on the basis that it is difficult to explain the intermediate state at an excitation energy of 2.3 MeV given by the opposite ordering. The 4_1^+ and 2_2^+ excitation energies predicted by the mean field calculations of Ref. [1] and the large scale shell model calculations of Ref. [6] all lie above 3 MeV. In the proposed level scheme, the 726, 1118, and 3430 keV γ rays deexciting the $J^\pi = (3^-)$ level at 4982 keV are most likely $E1$ transitions. The measured intensities of these γ rays and the nonobservation of an $E3$ transition to the ground state are consistent with the recommended upper limits on $B(E1)$ and $B(E3)$ values for the mass region [35]. Finally, the 2530 keV γ ray may correspond to the 2515.5 keV γ ray seen in coincidence with the $2_1^+ \rightarrow 0_{g.s.}^+$ transition in the β decay of ^{46}Cl [29]. On this basis, we tentatively place the 2530 keV transition directly above the 2_1^+ state.

We measured a cross section, corrected for feeding, of 11(2) mb for exciting the 2_1^+ state. The excitation cross section of the 3_1^- state, corresponding to the total cross section for producing the 3430, 1118, and 726 keV γ rays, was 4.5(11) mb. We did not observe γ rays on top of the 3_1^- state, so no feeding correction was made. Deformation lengths have been extracted from measured excitation cross sections using the coupled-channels code ECIS95 [36]. The thick-target method of inverse-kinematics proton scattering does not yield elastic-scattering angular distributions, and hence we are unable to determine optical potential parameters empirically. Instead, we have relied on a global nucleon-nucleus potential. Global potentials (see, for example, Refs. [37–39]) are based on measurements of stable nuclei for which proton angular distributions covering wide scattering-angle ranges are available. They have not been extensively tested for very neutron-rich nuclei. However, the global potential of Bechetti and Greenlees [37] has been successfully applied in studies of neutron-rich sulfur and argon isotopes [40,41]. The Bechetti-Greenlees potential is based on proton-scattering measurements with beam energies less than 50 MeV/nucleon and is therefore unsuitable for the present work. Instead, we have used the global potential of Koning and Delaroche [39], which is based on a larger set of measurements covering energies up to 200 MeV/nucleon. We find $\delta_2 = 0.88(9)$ fm for the $0_{g.s.}^+ \rightarrow 2_1^+$ excitation and $\delta_3 = 0.63(8)$ fm for the $0_{g.s.}^+ \rightarrow 3_1^-$ excitation using the vibrational model. Several theoretical studies [1–5] have indicated a shallow oblate minimum in the potential energy surface for ^{46}Ar at a deformation consistent with the quadrupole deformation $|\beta_2| = 0.186(13)$ measured via Coulomb excitation [13]. To

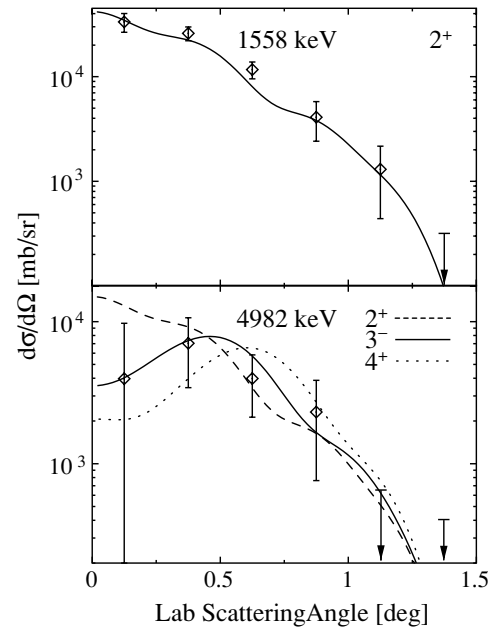


FIG. 4. Angular distributions of scattered ^{46}Ar particles measured in coincidence with γ rays deexciting the 2_1^+ and 3^- levels. Smooth curves are ECIS95 calculations described in the text.

account for a possible static quadrupole deformation, we performed a rotational-model calculation, which yielded a deformation length of $\delta_2 = 0.90(9)$ fm. The reduced radius of the real potential used in the ECIS calculations was $r_o = 1.19$ fm, giving quadrupole deformations of $\beta_2 = 0.206(20)$ and $|\beta_2| = 0.212(20)$ corresponding to the vibrational-model and rotational-model deformation lengths, respectively.

Laboratory-frame angular distributions of scattered ^{46}Ar particles measured in coincidence with γ rays deexciting the 2_1^+ level at 1558 keV and the 3^- level at 4982 keV are shown in Fig. 4. The 2_1^+ angular distribution was obtained from the yield of the 1558 keV γ ray measured in coincidence with each scattering-angle slice, corrected for feeding by subtraction of the yields of the 2307, 2530, 2692, and 3430 keV γ rays. The angular distribution for the 3^- level corresponds to the combined yields of the 3430 keV γ ray and the 1118–2307 keV and 726–2692 keV cascades, where the cascade yields were obtained by averaging the yields of the γ rays involved. Each data point corresponds to a slice of solid angle $d\Omega = 2\pi \sin\theta \Delta\theta$ with $\Delta\theta = 0.25^\circ$. The smooth curves in the figure are ECIS95 calculations smoothed to match the angular resolution of the S800 spectrograph. In the bottom panel, calculations assuming $J^\pi = 2^+, 3^-$, and 4^+ for the level at 4982 keV and giving the measured total cross section are included. The measured angular distribution is most consistent with our assignment of $J^\pi = 3^-$ to this level.

In the notation of Ref. [17], the deformation length measured using a probe F with a mixed sensitivity to protons and neutrons is related to the neutron and proton deformation lengths via

$$\delta_F = \frac{b_n^F N \delta_n + b_p^F Z \delta_p}{b_n^F N + b_p^F Z}, \quad (2)$$

where b_n^F (b_p^F) are the external-field neutron (proton) interaction strengths of the probe. Deformation lengths measured with a pair of experimental probes having different neutron and proton interaction strengths can be used to disentangle the neutron and proton deformation lengths δ_n and δ_p which in turn can be used to calculate the ratio of neutron to proton transition matrix elements M_n/M_p . An electromagnetic probe such as Coulomb excitation is sensitive only to protons ($b_n = 0$ and $b_p = 1$), giving $\delta_{EM} = \delta_p$. Following Bernstein *et al.* [16] for a case in which electromagnetic and proton-scattering deformation lengths are used, Eqs. (1) and (2) combine to give

$$\frac{M_n}{M_p} = \frac{b_p}{b_n} \left[\frac{\delta_{(p,p')}}{\delta_p} \left(1 + \frac{b_n N}{b_p Z} \right) - 1 \right]. \quad (3)$$

The ratio b_n/b_p is approximately 3 for proton scattering below 50 MeV and approximately 1 at 1 GeV [17], but it is not well determined at intermediate beam energies. Values of $(M_n/M_p)/(N/Z)$ for the 2_1^+ state of ^{46}Ar calculated assuming both $b_n/b_p = 1$ and $b_n/b_p = 3$ with the proton-scattering deformation lengths from the present work and the proton deformation length determined via Coulomb excitation from Ref. [13] are shown in Table II. The uncertainties given in the table reflect the experimental uncertainties in $\delta_{(p,p')}$ and δ_p . Including uncertainties, the results in Table II span the range $0.94N/Z \leq M_n/M_p \leq 1.44N/Z$. We adopt a value of $M_n/M_p = 1.19(25)N/Z$, which covers this range.

IV. DISCUSSION

Experimental results for the ratio of M_n/M_p to N/Z obtained with Eq. (3) and the absolute $B(E2, 0_1^+ \rightarrow 2_1^+)$ excitation strengths are compared to shell model calculations in Fig. 5. The $(M_n/M_p)/(N/Z)$ values for $A = 48-54$ are derived from electromagnetic deformation lengths from Ref. [14] and proton-scattering deformation lengths from Refs. [33] and [42]. The $B(E2 \uparrow)$ values are the adopted values from Ref. [14].

Shell model calculations were carried out with the harmonic-oscillator model space of pf for neutrons, sd for protons in ^{46}Ar , and pf for protons in $A = 50-54$, with the shell model codes OXBASH [43] ($A = 46, 48$) and MSHELL [44] ($A = 50, 52, 54$). For ^{46}Ar we use the sd - pf effective interaction developed in Ref. [45], and for $A = 48-54$ we use the pf GXPF1 effective interaction from Refs. [46,47].

The proton and neutron $E2$ matrix elements are obtained with the generalized effective charge model [48]; $M_p = A_p(1 + \delta_{pp}) + A_n\delta_{pn}$ and $M_n = A_n(1 + \delta_{nn}) + A_p\delta_{np}$, where

TABLE II. Values of $(M_n/M_p)/(N/Z)$ for the 2_1^+ state of ^{46}Ar calculated using the proton-scattering deformation lengths from the present work and the proton deformation length measured via Coulomb excitation from Ref. [13].

	$b_n/b_p = 1$	$b_n/b_p = 3$
Vibrational model	1.16(22)	1.12(16)
Rotational model	1.22(23)	1.16(17)

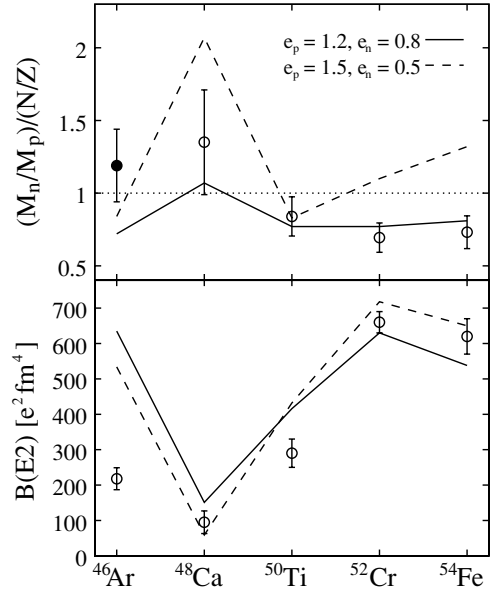


FIG. 5. Ratios of M_n/M_p to N/Z (top panel) and $B(E2; 0_{g.s.}^+ \rightarrow 2_1^+)$ values [14] (bottom panel) for the 2_1^+ states of even-even $N = 28$ isotones. The value of $(M_n/M_p)/(N/Z)$ for ^{46}Ar (\bullet) is from the present work, and those for $A = 48-54$ (\circ) are derived from deformation lengths given in Refs. [14,33,42]. The solid and dashed lines are shell model calculations described in the text.

A are the $E2$ matrix elements obtained in the model space, and δ_{cv} takes into account the polarization of the core nucleon c with the valence nucleon v . We assume effective charges appropriate for a ^{40}Ca core where from (N, Z) symmetry we have $\delta_{pp} = \delta_{nn} = e_p - 1$ and $\delta_{pn} = \delta_{np} = e_n$.

The model-space matrix elements A were obtained with harmonic-oscillator radial wave functions. Two sets of effective charges were used; $e_p = 1.5e$, $e_n = 0.5e$ and $e_p = 1.2e$, $e_n = 0.8e$. The former set is the standard isoscalar choice that can be related to the mixing of the isoscalar giant quadrupole resonance into the model-space wave functions. The latter set contains a significant isovector component related to mixing with the isovector giant quadrupole resonance [49] and is close to that suggested from a recent study of mirror nuclei in the pf shell [50].

As can be seen in the bottom panel of Fig. 5, the $B(E2 \uparrow)$ value from the shell model is rather insensitive to the set of effective charges used, while in the top panel, the ratio of the matrix elements shows a pronounced dependence and proves to be a valuable experimentally accessible quantity to study effective charges. The choice $e_p = 1.2e$ and $e_n = 0.8e$ clearly leads to a better description of the ratio of the matrix elements. However, the comparison of experimental and theoretical $B(E2 \uparrow)$ values reveals striking discrepancies for ^{46}Ar and ^{50}Ti (see Fig. 5) pointing to deficiencies of the present effective interactions which are most apparent in the structure of the two $N = 28$ isotones just two protons outside doubly magic ^{48}Ca . The smaller-than-expected $B(E2)$ values indicate that the coupling of the neutron excitations in ^{48}Ca is not as large as expected, perhaps an indication of a larger $\nu f_{7/2} - \nu p_{3/2}$ shell gap in ^{48}Ca than assumed in the models. A more detailed

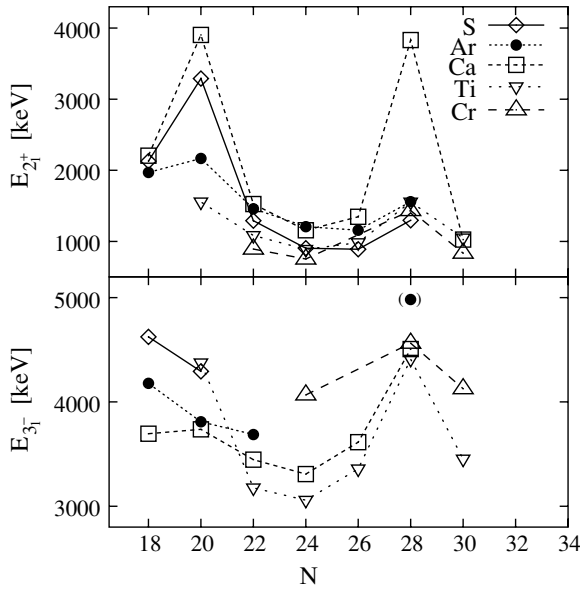


FIG. 6. Energies of the 2_1^+ states (top panel) and 3_1^- states (bottom panel) of even-even S, Ar, Ca, Ti, and Cr isotopes from Refs. [51–55] and the present work.

comparison with theory will require a microscopic calculation of the four core-polarization parameters δ_{cv} (and their orbital dependence) appropriate for a ^{48}Ca core.

The energies of the 2_1^+ states and 3_1^- states of the even-even neutron-rich S, Ar, Ca, Ti, and Cr isotopes are shown in Fig. 6 [51–55]. The 2_1^+ energies show a dramatic increase in the doubly magic nucleus ^{48}Ca flanked by a smaller, relatively uniform increase in the other $N = 28$ isotones, as expected based on the shell closures at $Z = 20$ and $N = 28$. The $E_{3_1^-}$ energies in ^{48}Ca , ^{50}Ti , and ^{52}Cr fall within a very narrow range centered at about 4500 keV, with no distinguishing increase at $Z = 20$. This can be explained in terms of the details of the shell structure. The 3_1^- states of the $N = 28$ isotones with $Z \geq 20$ must be primarily proton excitations

because of the large energy required to promote $f_{7/2}$ neutrons to the $g_{9/2}$ intruder orbit. There is experimental evidence that the 3_1^- states of ^{48}Ca and ^{50}Ti are primarily $(\pi s_{1/2})^{-1}(\pi f_{7/2})$ excitations [31,33]. This would explain the similar 3_1^- energies of these nuclei. Moreover, the assumption that $1p-1h$ proton excitations to the $f_{7/2}$ shell dominate in the neutron-rich $N = 28$ isotones is consistent with the increase in the fragmentation of low-lying octupole strength with increasing Z (increasing $f_{7/2}$ occupancy) observed in the proton-scattering study of Ref. [31]. We have tentatively identified the 3_1^- state of ^{46}Ar at 4982 keV with a deformation length of $\delta_3 = 0.63(8)$, similar to those of the 3_1^- states of neighboring $N = 28$ isotones ^{48}Ca , ^{50}Ti , and ^{52}Cr which fall between $\delta_3 = 0.61$ and $\delta_3 = 0.76$ [31,33]. The excitation energy of this state lies about 500 keV above those of the neutron-rich even-even $N = 28$ isotones with $Z \geq 20$, indicating a change in the underlying configuration of the 3_1^- state with the removal of two protons from the $Z = 20$ shell.

V. SUMMARY

We have studied low-lying states of ^{46}Ar via thick-target inverse-kinematics proton scattering. The deformation length of the $0_{g.s.}^+ \rightarrow 2_1^+$ excitation has been measured and combined with the most recent Coulomb excitation result to obtain a value of $M_n/M_p = 1.19(25)N/Z$ indicating a greater neutron contribution to this excitation than in those of the $N = 28$ isotones above ^{48}Ca . This result is consistent with a quadrupole-deformed ground state. Although the spherical shell at $N = 28$ may vanish below ^{48}Ca , the systematic behavior of the known two-neutron separation energies and 2_1^+ state energies in this region indicate a persistent $\nu f_{7/2}-\nu p_{3/2}$ energy gap.

ACKNOWLEDGMENT

This work was supported by the National Science Foundation under Grant Nos. PHY-0110253, PHY-0244453, PHY-0342281, and PHY-0355129.

- [1] R. Rodríguez-Guzmán, J. L. Egidio, and L. Robledo, *Phys. Rev. C* **65**, 024304 (2002).
- [2] B. V. Carlson and D. Hirata, *Phys. Rev. C* **62**, 054310 (2000).
- [3] S. Péru, M. Girod, and J. F. Berger, *Eur. Phys. J. A* **9**, 35 (2000).
- [4] G. A. Lalazissis, D. Vretenar, P. Ring, M. Stoitsov, and L. M. Robledo, *Phys. Rev. C* **60**, 014310 (1999).
- [5] T. R. Werner, J. A. Sheikh, M. Misu, W. Nazarewicz, J. Rikovska, K. Heeger, A. S. Umar, and M. R. Strayer, *Nucl. Phys.* **A597**, 327 (1996).
- [6] E. Caurier, F. Nowacki, and A. Poves, *Nucl. Phys.* **A742**, 14 (2004).
- [7] E. Caurier, F. Nowacki, and A. Poves, *Eur. Phys. J. A* **15**, 145 (2002).
- [8] D. J. Dean, M. T. Ressel, M. Hjorth-Jensen, S. E. Koonin, K. Langanke, and A. P. Zuker, *Phys. Rev. C* **59**, 2474 (1999).
- [9] J. Retamosa, E. Caurier, F. Nowacki, and A. Poves, *Phys. Rev. C* **55**, 1266 (1997).
- [10] O. Sorlin, D. Guillemaud-Mueller, A. C. Mueller, V. Borrel, S. Dogny, F. Pougheon, K.-L. Kratz, H. Gabelmann, B. Pfeiffer, A. Wöhr *et al.*, *Phys. Rev. C* **47**, 2941 (1993).
- [11] M. Lewitowicz, Y. E. Penionzhkevich, A. G. Artukh, A. M. Kalinin, V. V. Kamanin, S. M. Lukyanov, N. H. Chau, A. C. Mueller, D. Guillemaud-Mueller, R. Anne *et al.*, *Nucl. Phys.* **A496**, 477 (1989).
- [12] T. Glasmacher, B. A. Brown, M. J. Chromik, P. D. Cottle, M. Fauerbach, R. W. Ibbotson, K. W. Kemper, D. J. Morrissey, H. Scheit, D. W. Sklenicka *et al.*, *Phys. Lett.* **B395**, 163 (1997).
- [13] A. Gade, D. Bazin, C. M. Campbell, J. A. Church, D. C. Dinca, J. Enders, T. Glasmacher, Z. Hu, K. W. Kemper, W. F. Mueller *et al.*, *Phys. Rev. C* **68**, 014302 (2003).

- [14] S. Raman, J. C. W. Nestor, and P. Tikkanen, *At. Data Nucl. Data Tables* **36**, 1 (2001).
- [15] H. Scheit, T. Glasmacher, B. A. Brown, J. A. Brown, P. D. Cottle, P. G. Hansen, R. Harkewicz, M. Hellström, R. W. Ibbotson, J. K. Jewell *et al.*, *Phys. Rev. Lett.* **77**, 3967 (1996).
- [16] A. M. Bernstein, V. R. Brown, and V. A. Madsen, *Comments Nucl. Part. Phys.* **11**, 203 (1983).
- [17] A. M. Bernstein, V. R. Brown, and V. A. Madsen, *Phys. Lett.* **B103**, 255 (1981).
- [18] M. A. Kennedy, P. D. Cottle, and K. W. Kemper, *Phys. Rev. C* **46**, 1811 (1992).
- [19] R. Anne, D. Bazin, R. Bimbot, M. J. G. Borge, J. Corre, S. Dogny, S. Emling, D. Guillemaud-Mueller, P. G. Hansen, P. Hornshj *et al.*, *Z. Phys. A* **352**, 397 (1995).
- [20] T. Glasmacher, *Annu. Rev. Nucl. Part. Sci.* **48**, 1 (1998).
- [21] G. Kraus, P. Egelhof, C. Fischer, H. Geissel, A. Himmler, F. Nickel, G. Münzenberg, W. Schwab, A. Weiss, J. Friese *et al.*, *Phys. Rev. Lett.* **73**, 1773 (1994).
- [22] J. H. Kelley, T. Suomijärvi, S. E. Hirzebruch, A. Azhari, D. Bazin, Y. Blumenfeld, J. A. Brown, P. D. Cottle, S. Danczyk, M. Fauerbach *et al.*, *Phys. Rev. C* **56**, R1206 (1997).
- [23] H. Iwasaki, T. Motobayashi, H. Akiyoshi, Y. Ando, N. Fukuda, H. Fujiwara, Z. Fülöp, K. I. Hahn, Y. Higurashi, M. Hirai *et al.*, *Phys. Lett.* **B481**, 7 (2000).
- [24] D. J. Morrissey, B. M. Sherrill, M. Steiner, A. Stolz, and I. Wiedenhöver, *Nucl. Instrum. Methods Phys. Res. B* **204**, 90 (2003).
- [25] D. Bazin, J. A. Caggiano, B. M. Sherrill, J. Yurkon, and A. Zeller, *Nucl. Instrum. Methods Phys. Res. B* **204**, 629 (2003).
- [26] W. F. Mueller, J. A. Church, T. Glasmacher, D. Gutknecht, G. Hackman, P. G. Hansen, Z. Hu, K. L. Miller, and P. Quirin, *Nucl. Instrum. Methods Phys. Res. A* **466**, 492 (2001).
- [27] GEANT version 3.21, CERN program library, long writeup W5013 (1994).
- [28] Z. Dombrádi, D. Sohler, O. Sorlin, F. Azaiez, F. Nowacki, M. Stanoiu, Y.-E. Penionzhkevich, J. Timár, F. Amorini, D. Baiborodin *et al.*, *Nucl. Phys.* **A727**, 195 (2003).
- [29] J. Mrázek, S. Grévy, S. Iulian, A. Buta, F. Negoita, J. C. Angélique, P. Baumann, C. Borcea, G. Canchel, W. Catford *et al.*, *Nucl. Phys.* **A734**, E65 (2004).
- [30] B. Fornal, R. Broda, W. Krolas, T. Pawlat, J. Wrzesinski, D. Bazzacco, S. Lunardi, C. R. Alvarez, G. Viesti, G. de Angelis *et al.*, *Eur. Phys. J. A* **7**, 147 (2000).
- [31] M. Fujiwara, Y. Fujita, S. Imanishi, S. Morinobu, T. Yamazaki, H. Ikegami, K. Katori, and S. I. Hayakawa, *Phys. Rev. C* **32**, 830 (1985).
- [32] M. Fujiwara, S. Morinobu, M. Tosaki, H. Ito, I. Katayama, H. Ikegami, S. I. Hayakawa, N. Ikeda, H. Ohsumi, A. Higashi *et al.*, *Phys. Rev. C* **35**, 1257 (1987).
- [33] Y. Fujita, M. Fujiwara, S. Morinobu, T. Yamazaki, T. Itahashi, H. Ikegami, and S. I. Hayakawa, *Phys. Rev. C* **37**, 45 (1988).
- [34] A. Higashi, K. Katori, M. Fujiwara, H. Ikegami, I. Katayama, S. Morinobu, M. Tosaki, S. I. Hayakawa, N. Ikeda, and H. Miyatake, *Phys. Rev. C* **39**, 1286 (1989).
- [35] P. M. Endt, *At. Data Nucl. Data Tables* **23**, 547 (1979).
- [36] J. Raynal, Notes on ECIS94, Note CEA-N-2772 (1994).
- [37] F. D. Bechetti, Jr., and G. W. Greenlees, *Phys. Rev.* **182**, 1190 (1969).
- [38] R. L. Varner, W. J. Thompson, T. L. McAbee, E. J. Ludwig, and T. B. Clegg, *Phys. Rep.* **201**, 57 (1991).
- [39] A. J. Koning and J.-P. Delaroche, *Nucl. Phys.* **A713**, 231 (2003).
- [40] F. Maréchal, T. Suomijärvi, Y. Blumenfeld, A. Azhari, E. Bauge, D. Bazin, J. A. Brown, P. D. Cottle, J. P. Delaroche, M. Fauerbach *et al.*, *Phys. Rev. C* **60**, 034615 (1999).
- [41] H. Scheit, F. Maréchal, T. Glasmacher, E. Bauge, Y. Blumenfeld, J. P. Delaroche, M. Girod, R. W. Ibbotson, K. W. Kemper, J. Libert *et al.*, *Phys. Rev. C* **63**, 014604 (2000).
- [42] V. A. Madsen, V. R. Brown, and J. D. Anderson, *Phys. Rev. C* **12**, 1205 (1975).
- [43] B. A. Brown *et al.*, OXBASH for windows, MSU-NSCL Report 1289 (2004).
- [44] T. Mizusaki, *RIKEN Accel. Prog. Rep.* 33 (2000).
- [45] S. Nummela, P. Baumann, E. Caurier, P. Dessagne, A. Jokinen, A. Knipper, G. L. Scornet, C. Miehè, F. Nowacki, M. Oinonen *et al.*, *Phys. Rev. C* **63**, 044316 (2001).
- [46] M. Honma, T. Otsuka, B. A. Brown, and T. Mizusaki, *Phys. Rev. C* **65**, 061301(R) (2002).
- [47] M. Honma, T. Otsuka, B. A. Brown, and T. Mizusaki, *Phys. Rev. C* **69**, 034335 (2004).
- [48] B. A. Brown and B. H. Wildenthal, *Phys. Rev. C* **21**, 2107 (1980).
- [49] B. A. Brown, A. Arima, and J. B. McGrory, *Nucl. Phys.* **A277**, 77 (1977).
- [50] R. du Rietz, J. Ekman, D. Rudolph, C. Fahlander, A. Dewald, O. Möller, B. Saha, M. Axiotis, M. A. Bentley, C. Chandler *et al.*, *Phys. Rev. Lett.* **93**, 222501 (2004).
- [51] J. A. Cameron and B. Singh, *Nucl. Data Sheets* **88**, 299 (1999).
- [52] S.-C. Wu, *Nucl. Data Sheets* **91**, 1 (2000).
- [53] T. W. Burrows, *Nucl. Data Sheets* **68**, 1 (1993).
- [54] T. W. Burrows, *Nucl. Data Sheets* **75**, 1 (1995).
- [55] H. Junde, *Nucl. Data Sheets* **90**, 1 (2000).